Volume 1 | Number 1 | Jan 2013 | Pages 1–100

Journal of
Materials Chemistry A

Materials for energy and sustainability
www.rsc.org/materialsA

ROYAL SOCIETY OF CHEMISTRY

www.rsc.org/materialsA

Journal Name

ARTICLE

Structure and Function Relationships in Alkylammonium Lead(II) Iodide Solar Cells

Majid Safdari[a], Andreas Fischer[a], Bo Xu[b], Lars Kloo[a] and James Gardner[a]*

Alkylammonium lead(II) iodide materials ($APbI_3$), based on the general formula of CH_3-$(CH_2)_n$-NH_3PbI_3, may lead to a monumental leap in developing affordable photovoltaics. Herein, we correlate the structure and function relationships of alkylammonium lead(II) iodide in solar cells. We investigated changes in the structure of $APbI_3$ materials by varying the alkylammonium cations in their structure. As the size of the alkylammonium cation increased, the crystallographic unit cell increased in size and yielded lower symmetry crystals. High symmetry materials, those with cubic symmetry, showed the highest conductivity, the smallest bandgap, and produced the best performing solar cells. Structural changes were investigated by X-ray crystallography, X-ray powder diffraction, and Raman scattering.

Introduction

Solid-state dye-sensitized solar cells (ssDSCs) are making substantial progress as an alternative to conventional dye-sensitized solar cells. The highest recorded efficiency for ssDSCs utilizing an organic photosensitizer and the hole transporting material Spiro-OMeTAD (2,2',7,7'-tetrakis(N,N-di-p-methoxyphenylamino)-9,9'-spirobifluorene) was 7.2%.[1] Though impressive, this result is still lower than record for the conventional DSCs based on a liquid electrolyte.[2] A revolution in solid-state solar cells was initiated by employing methylammonium lead(II) halides ($MAPbX_3$) as photosensitizers and hole-transporting materials in mesoscopic solar cells.[3, 4] The $MAPbX_3$ materials have several properties that make them interesting for use as light harvesting and charge-transporting components in solar cells, e.g direct band gap, large extinction coefficients,[5] high carrier mobility,[4, 6, 7] and the ease of solution processing. Another inherent key property of the $MAPbX_3$ materials is most likely related to their tendency to generate a material with few bulk and surface defects, even inside a mesoporous metal oxide host.[8, 9] Finding other solution processed materials that can improve upon present material properties and show reasonably decent function in combination with other components in the solar cell represents a challenge in this field.[10, 11] Mesoscopic solar cells based upon methylammonium lead(II) iodide as a light absorber have shown major progress during the last two years and are presently over 16% power conversion efficiency.[3, 4, 7, 12-14] Prior to their use in ssDSC, $MAPbX_3$ quantum dots were utilized as light absorbing materials in liquid-based DSC.[15, 16] However, these types of solar cells showed low stability due to the dissolution of methylammonium iodide into the electrolyte solution resulting in rapid loss in solar cell function. Changing from liquid electrolyte to solid hole transporting material was a very significant development in this field. Recently, perovskite thin film solar cells based on

methylammonium lead(II) halide, as light absorber, in combination with Spiro-OMeTAD, as a hole transport material, have shown remarkable performance.[7, 12, 17] To further improve on solar cells based on alkylammonium lead(II) halides, $APbX_3$, it is necessary to understand the fundamental properties from which they derive their function. In the present work, we investigate the effect of crystal structure on the electronic properties of the materials by varying the alkylammonium cation size. As mentioned elsewhere,[18] ideal perovskites are metal oxides with a cubic structure and a formal composition AMX_3, where A and M are cations in two crystallographically different positions, A positioned in the unit cell cube corners and M positioned in the cube center, and X is positioned at the center of each unit cell edge. Methylammonium lead(II) halides have a perovskite crystal structure. In the perovskites of interest to solar cells, A is an arbitrary monovalent cation, M is a main-group element, such as tin or lead, and X is a halogen. Many of the materials of interest also significantly deviate from the ideal perovskite structure in terms of both structure and composition; in the latter case, typically the amount of X is higher giving rise to layered, perovskite-like structures of the Mitzi type.[19-21] The perovskite structure can be regarded as consisting of layers along different crystallographic directions, and several possible orientations can be considered, eg. <100>, <110> and <111>. Perovskite-like structures typically consist of layers of corner-sharing metal halide octahedra. The structure of these AMX_3 materials represents an interesting platform for structure-property modifications, where the layered structure motif offers sufficient flexibility for modifications and can be amended through the changing of the composition of the different components in the precursor solutions. One can change the halide anion, which leads to different materials with a range of bandgaps, although with a conserved perovskite crystal structure.[22, 23] On the other hand, as shown in this work, changing the organic cation has remarkable

effect on the structure of the material, which would be beneficial for increasing our knowledge about the structure and function relationship of these materials. In this work, we have prepared three APbI$_3$ materials and varied the alkylammonium as cation chain length. We fabricated methylammonium iodide, ethylammonium iodide and propylammonium iodide and used them to prepare APbI$_3$ materials with the respective alkylammonium cations. The synthesized materials were methylammonium lead(II) iodide (MAPbI$_3$), ethylammonium lead(II) iodide (EAPbI$_3$) and propylammonium lead(II) iodide (PAPbI$_3$). It is proposed that the organic cation in this structure does not have a major role in the electronic band structure and strictly maintains the neutrality of the crystal lattice, while the band structure is dependent on the lead halide anion structure.[24] However, the size of cation is very important in determining the three-dimensional structure of the material. We have focused on the effect of this change in order to obtain fundamental information about the materials and connect it to the performance of the solar cells based on these materials.

Experimental

Material synthesis: All chemicals were purchased from Sigma-Aldrich unless otherwise stated. Alkylammonium lead(II) iodide materials (APbI$_3$) were prepared according to the procedure used elsewhere[3, 16] and are summarized briefly below. To prepare each alkylammonium iodide, hydroiodic acid (15 mL of 57 wt. % in water) was mixed and stirred with the relevant alkylamine (13.9 mL of 40% methyl amine in methanol, 10.8 mL of 70% ethylamine in water, and 11.2 mL of propylamine >99%) at 0°C for two hours. The resulting solution was evaporated and washed three times with diethyl ether and then dried under vacuum for 12 hours at 60°C.

For the synthesis of APbI$_3$, 1:1 molar ratios of the alkylammonium salt and PbI$_2$ (99.999%) at a concentration of 0.013 M were dissolved in dimethylformamide (anhydrous, 99.8%) at 60 °C overnight. The solution was filtered (if any precipitation occurred) through a PTFE syringe filter 0.45 μm pore size. Sample powder was recovered by evaporation of the solvent at 50 °C. All of the synthesis processes were performed under ambient air.

Characterizations: A 40 wt % solution of the APbI$_3$ materials was used to spin coat the materials onto a microscope slide covered by a 2μm layer of TiO$_2$. This was followed by heating at 100 °C. UV-Visible absorption spectra were recorded using UV-Visible Cary 300 spectrophotometer.

Solutions containing 400 mg/ml of the APbI$_3$ samples in γ-Butyrolactone (Reagent Plus® >99%) were used for single crystal growth. The solutions were heated to 100 °C and were kept at this temperature for 30 minutes. The solutions were then cooled very slowly (3 °C/h). Crystal growth started at 75 °C. For MAPbI$_3$ samples, crystals were stable at temperature higher than 55 °C due to its phase transition at 55 °C from cubic (at higher than 55 °C) to tetragonal (at lower than 55 °C). For PAPbI$_3$, stable crystals were obtained at room temperature.[18] Single crystals of methylammonium lead(II) iodide and propylammonium lead(II) iodide (shown using a compound optical microscope in Figure 3) were used for the collection of data at 323 K. Diffraction data were collected on a Bruker-Nonius KappaCCD diffractometer. Absorption corrections based on multiple scans (SADABS) were applied.[25] The structures were solved using direct methods and refined on F$_2$ with anisotropic thermal parameters for all non-H atoms.[26] H atoms were refined on calculated positions using a riding model. Table 1 summarizes the results of the structure determinations. Despite our best efforts, single crystals of EAPbI$_3$ could not be grown in our hands.

Samples were ground in a mortar before collecting powder X-ray diffraction patterns. We investigated the recovered powders of the APbI$_3$ materials by X-ray diffraction, PANalytical-X'Pert PRO diffractometer using Cu-Kα radiation, and scanned over a 2θ range of 10° to 40°.

Raman spectra of well-ground APbI$_3$ powders were acquired on a BioRad FTS 6000 spectrometer equipped with a Raman accessory using a quartz beamsplitter, 4 cm^{-1} resolution and a nitrogen cooled Ge detector.

In order to measure the electrical conductivity, samples were prepared as follows and as shown in Figure 1. A 600 nm layer of mesoporous TiO$_2$ was deposited onto a non-conductive glass substrate, APbI$_3$ materials were then spin coated into the TiO$_2$ layer and lastly, on the top, two thin layers of silver 2 cm wide were deposited. The photocurrent was measured when a bias voltage from -1 V to 1 V was applied across the two silver layers. The inverse of the slope obtained from the current-voltage curve is the film resistance, R.[1] The electrical conductivity (σ) was calculated by using the following equation (1):

$$\sigma = \frac{W}{R.L.d} \quad (1),$$

where W is the width between adjacent silver channels, d is the depth of the APbI$_3$/TiO$_2$ film corrected for the TiO$_2$ volume, and L is the length Ag film. The TiO$_2$ films have 60% porosity. To correct for the volume of the TiO$_2$, the thickness of the materials (d) was multiplied by 60%.
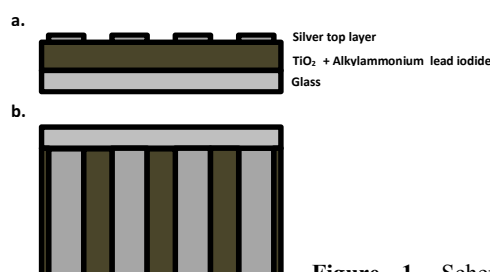
Figure 1. Schematic a. cross-sectional view and b. top view diagram of the devices used for the conductivity measurement.

Solar cell preparation: The FTO-glass was cleansed by washing in an ultrasonic bath containing a solution of 2 wt% detergent. Cleaning was continued in an ultrasonic bath containing ethanol and then acetone. To make a compact TiO$_2$ blocking layer, the cleansed FTO substrates were heated to 500°C, then a solution of 2 M titanium isopropoxide in propanol was spray pyrolyzed onto the FTO. The mesoporous TiO$_2$ layer was prepared by spin coating of TiO$_2$ on the substrate at 3000 rpm spinning rate. Films were then sintered at 500 °C for 30 minutes. Sintered films were immersed into a 40 mM solution of TiCl$_4$ in water for 30 minutes at 70 °C. Lastly the TiO$_2$ films were sintered at 500°C for 30 minutes. DMF solutions with 40 wt % of APbI$_3$ samples were used. Materials were spin coated (at 1500 rpm spinning rate) into the TiO$_2$ mesoporous layer followed by annealing to 100 °C for 5 minutes. The hole transporting material (HTM) solution contained 0.08 M Spiro-OMeTAD (2,2',7,7'-tetrakis(N,N-di-p-methoxyphenylamino)-9,9'-

spirobifluorene, 99.99%, Lumtec), 0.03 M bis(trifluoromethane) sulfonimide lithium salt (LiTFSI, 99%, Io-li-tec) and 0.198 M 4-tert-butylpyridine (TBP, 99%). A mixture of 10 wt % acetonitrile (99.8%) and 90 wt % chlorobenzene (99.8%) was used as solvent for hole transporting material solution. Spin coating of the HTM solution was performed at 2000 rpm. Finally, a 200 nm thick layer of silver was deposited on top of the HTM layer as a counter electrode.[3, 7] All of the solar cell fabrication steps were performed in ambient air and at ambient temperature, except for the final silver evaporation process to generate the counter electrode.

Results and discussion

UV-Visible measurement: All of the samples showed absorption edges in either the near-IR and visible regions that correspond to the energy gap between the valence band and conduction band, Figure 2.
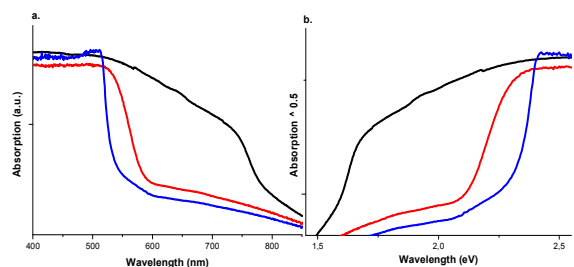
Figure 2. a. Absorption spectra and b. Tauc plot of the --- $(CH_3NH_3)PbI_3$,---$(CH_3CH_2NH_3)PbI_3$,and --- $(CH_3CH_2CH_2NH_3)PbI_3$.

For the calculation of the bandgap the Tauc equation was used, equation (2).[27]

$$(\alpha h\nu)^{1/n} = A(h\nu - E_g) \quad (2),$$

Table 1 Calculated bandgap for the $APbI_3$ materials using Tauc equation for direct bandgap transitions.

$APbI_3$	Bandgap(eV)
$CH_3NH_3PbI_3$	1.6
$CH_3CH_2NH_3PbI_3$	2.2
$CH_3CH_2CH_2NH_3PbI_3$	2.4

Where h is Planck constant, ν is the frequency, α is the absorption coefficient, E_g is the bandgap and A is a normalization constant. For a direct electronic transition, as is observed in the $APbI_3$ materials, the bandgap is calculated to be the abscissa intercept on a plot of $(\alpha h\nu)^{1/2}$ vs $h\nu$. For $MAPbI_3$ a band edge was detected at 785 nm; this is equivalent to a bandgap of 1.6 eV, which is in agreement with other studies.[18] While for $EAPbI_3$ this value has been shifted to 568 nm, corresponding to a bandgap of 2.2 eV. For PAPbI3, a higher shift was detected to 523 nm, corresponding to a bandgap of 2.4 eV. As it is shown in the Figure 2, the $APbI_3$ materials containing bulkier alkylammonium groups have absorption onsets that are shifted to shorter wavelengths. It can be concluded

that by changing to a bulkier cation, from methyl to propyl, the distance between PbI_6^{4-} structural units increases; this leads to decreased orbital overlap and lower absorption in the visible region of the spectrum.

Powder X-ray diffraction: The obtained diffractograms are shown in Figure 3. The indices for $MAPbI_3$ and $EAPbI_3$ were taken from literature values and matched well with our data.[18, 28, 29] The indices for $PAPbI_3$ were taken from our single crystal data (shown below in Figure 6). The powder patterns show that all of the $APbI_3$ materials are polycrystalline and are a single phase. When comparing the three $APbI_3$ materials, there does not appear to be a strong correlation between the calculated Miller indices for the powder patterns and the peak positions. There is substantial anisotropy in the powder pattern for $PAPbI_3$; many of the peaks predicted from single crystal data are supressed. Since the powders more closely relate to materials present in the solar cells, this bias in orientation may be present in solar cells made using $PAPbI_3$ as well. However, since the high Z-number elements Pb and I dominate the powder X-ray pattern, the patterns only produce indirect information on the less massive alkylammonium groups. To further refine these conclusions, we grew single crystals of $MAPbI_3$ and $PAPbI_3$.
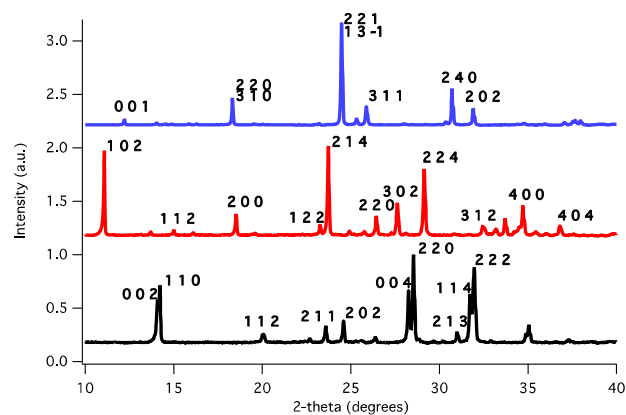
Figure 3. Powder X-ray diffraction patterns of --- $(CH_3NH_3)PbI_3$, --- $(CH_3CH_2NH_3)PbI_3$, and --- $(CH_3CH_2CH_2NH_3)PbI_3$.

Single-crystal X-ray diffraction: The crystallographic data for the refined structures are presented in Table 2.
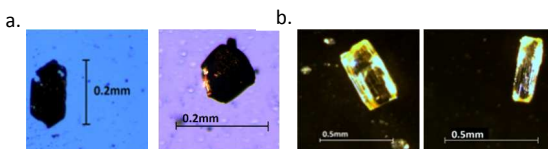
Figure 4. Compound optical microscope images of (a) methylammonium lead (II) iodide, $MAPbI_3$ and (b) propylammonium lead(II) iodide, $PAPbI_3$ crystals used for single crystal X-ray diffraction.

The refined crystal structures of the samples are presented in Figures 5 and 6 for methylammonium lead(II) iodide and propylammonium lead(II) iodide, respectively. The data for crystal

structure of the ethylammonium lead(II) iodide was extracted from a report by Park et al.[29]

Table 2 Refined structural details of methylammonium lead(II) iodide and propylammonium lead(II) iodide. Ethylammonium lead(II) iodide structural details were reported by Park et al.[29]

	MAPbI$_3$	EAPbI$_3$ [29]	PAPbI$_3$ + C$_4$H$_6$O$_2$	
Space group	P m -3 m	Pmmn	C c	
Cell lengths (Å)	a 6.284	a 8.742	a 17.770	
	b 6.284	b 8.147	b 12.380	
	c 6.284	c 30.310	c 8.071	
Cell angles	α 90.00	α 90.00	α 90.00	
	β 90.00	β 90.00	β 116.77	
	γ 90.00	γ 90.00	γ 90.00	
Cell volume (Å^3)		248.15	2158.78	1585.26
Z		1	8	4

In agreement with literature, MAPbI$_3$ has a cubic structure with a space group of Pm-3m.[18] The exact positions of the atoms in the methylammonium group was not obtained from the crystal structure determination because of a combination between the large difference in electron density with respect to lead and iodine, and because of dynamic or static disorder in the crystal lattice. In this structure, the distances between lead atoms are equal and unit cells are corner sharing in all three dimensions, Figure 5. The distance between lead atoms is 6.284 Å in all three dimensions with an ideal angle of 180° for Pb-I-Pb and 90° between I-Pb-I. Park et al[29] report on the structural analysis of EAPbI$_3$ and declare an orthorhombic structure in the space group of Pmmn. The single crystals of PAPbI$_3$ reveal a solvate that incorporates a single GBL molecule into the structure. A monoclinic structure in the space group of Cc was found for the PAPbI$_3$ solvate. For EAPbI$_3$ and PAPbI$_3$, the bulkier cation leads to a structure that is not corner-sharing, but is instead face-sharing in only one dimension. A one dimensional chain was found for both lead iodide units in EAPbI$_3$ and PAPbI$_3$. A larger distance between structural lead iodide units was observed as compared to MAPbI$_3$. For EAPbI$_3$ the distances between the lead atoms within one chain are observed in the range of 3.648 to 4.499 Å and between the chains they are observed at 8.804 Å. For PAPbI$_3$ lead atom-atom distances within the chain and between the chains are 4.036 Å and 10.829 Å, respectively. In EAPbI$_3$, the I-Pb-I angles varies between 172.02 and 178.83 degrees and in PAPbI$_3$ same angles fluctuates from 175.88 to 178.42. Unlike in MAPbI$_3$, which has linear Pb-I-Pb angles, the angles for Pb-I-Pb in PAPbI$_3$ are between 77.04 and 77.85 degrees. This change in Pb-I-Pb angle is due to the shift from corner-sharing octahedra in MAPbI$_3$ to face-sharing octahedra in PAPbI$_3$. The Pb to Pb distance through Pb-I bonds in EAPbI$_3$ varies between 6.050 and 6.858 Å, which is on average longer than the distances between Pb atoms in MAPbI$_3$ (6.284 Å). The same phenomenon is observed for PAPbI$_3$, where the distance varied between 6.423 and 6.479 Å. The noticeable increase of the distances between lead iodide structural

units has proved that upon changing the cation from methylammonium to the bulkier propylammonium cation the interaction between the main structural units is reduced. The bigger cation occupies a larger space between the lead iodide units and is an obstacle to forming corner-sharing units in all three dimensions. As it can be seen in the Figure 6, the structure of PAPbI$_3$ is a one dimensional PbI$_3$ chain due to the occupation of a larger volume by the cation. This bigger space between lead iodide units even facilitates solvent incorporation into the structure. As mentioned above, the unit cells for PAPbI$_3$ incorporate γ-butyrolactone as a structural feature.
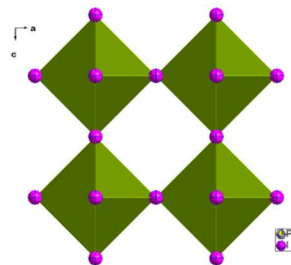
Figure 5. Methylammonium lead(II) iodide (MAPbI$_3$) crystal structure shown at a 50% probability level.
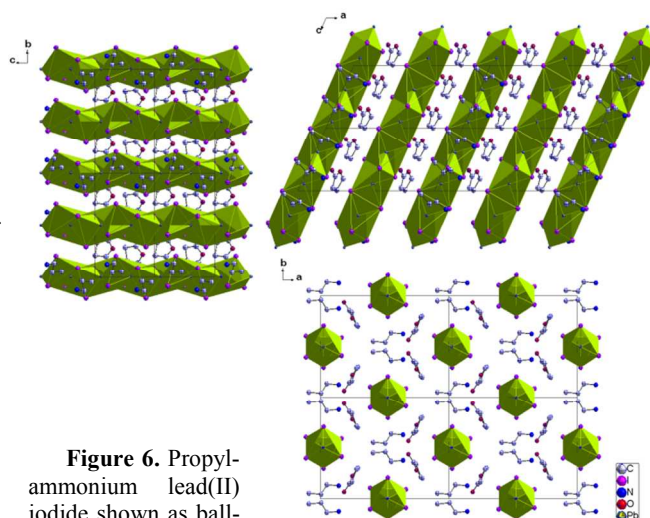
Figure 6. Propylammonium lead(II) iodide shown as ball-and-stick models for simplicity along the three different axes.

As shown from the crystal structure of the materials, the cation is embedded in the void between the lead iodide structural units, which are sharing octahedral faces. The bulkiness of the cations clearly increases the distance between lead iodide structural units in two out of three dimensions, and it significantly changes the structure of the materials as was shown by Mitzi and coworkers for related materials.[19, 21]

Raman spectroscopy: The obtained Raman spectra are shown in Figure 7. For all samples, an intense peak was observed at ~120 cm^{-1}, which is attributable to the Pb-I bond vibration.[30] In the ideal and three-dimensional case, the fundamental vibrational mode that is responsible for the strongest Raman signal originates from the triply degenerate (along the three crystallographic directions in the cubic

AMI$_3$ structure), asymmetric I-Pb-I (or Pb-I-Pb) stretch. For MAPbI$_3$, EAPbI$_3$, and PAPbI$_3$ samples this peak was observed at 131 cm^{-1}, 113 cm^{-1}, and 115 cm^{-1} respectively. In EAPbI$_3$ and PAPbI$_3$, the I-Pb-I angle is less than 90 degrees and the Pb-I distances are greater than in MAPbI$_3$. This qualitatively matches well with Raman data, which indicate that the Pb-I bond order decreases in EAPbI$_3$ and PAPbI$_3$. We attribute this as the main reason for the shifting the Pb-I vibration to the lower frequency. All of the Pb-I bond lengths in the cubic MAPbI$_3$ are 3.14 Å. This can be compared to EAPbI$_3$, which has Pb-I bond lengths in the range of 3.025 to 3.429 Å (average 3.246Å). For PAPbI$_3$, Pb-I bond lengths are in the range of 3.20 Å to 3.25 Å (average 3.228Å) (Table S3). It is notable that the largest difference is seen when going from the MA to the EA cation. Of course, because of the difference in linkage between the PbI$_6$ octahedra in the three different compounds, also differences in effective mass can play a role.

Concluded from single crystal data of the PAPbI$_3$, it was discussed that due to bulky size of cation the solvent is present in the crystal structure. Sample powders were recovered from dimethylformamide solution of the compounds. By comparing the Raman spectra of PAPbI$_3$ and dimethylformamide,[31] it is clear that dimethylformamide is present in the sample powder of PAPbI$_3$. Detected peaks at 667 cm^{-1}, 866 cm^{-1}, and 1413 cm^{-1} are marked by a red arrow in the spectrum of PAPbI$_3$. These peaks may be weakly observed in the EAPbI$_3$ spectrum and are not present in the spectrum of MAPbI$_3$. Observed peaks between 1400 cm^{-1} to 1700 cm^{-1} are attributed to the $\delta(CH_2)$ and $\delta(CH_3)$. Primary amine peaks related to vibrations of N-H bond have been observed at 3000 cm^{-1}. These peaks have been identified in Raman spectra of the alkylammonium salt as well as in spectra of alkylammonium lead(II) iodide (See Figures S1, S2 and S3).
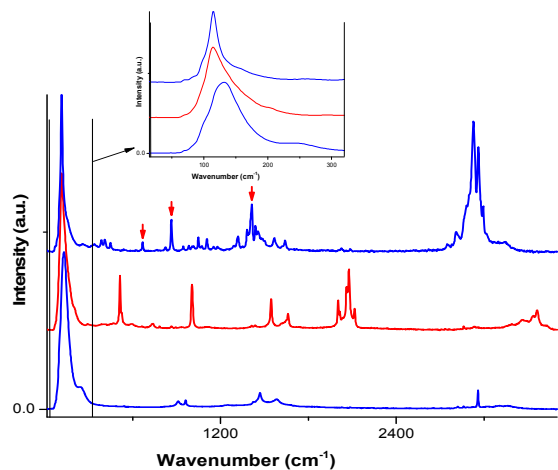
Figure 7. a. Raman spectra of --- (CH$_3$NH$_3$)PbI$_3$, --- (CH$_3$CH$_2$NH$_3$)PbI$_3$, and --- (CH$_3$CH$_2$CH$_2$NH$_3$)PbI$_3$b. Magnification of the low frequency vibrations attributed to Pb-I structural units.

Solar cell data: Solar cells were prepared based on the three APbI$_3$ materials as photosensitizers; all of the other components were same for the solar cells. Figure 8 shows the related curves of current density-voltage (IV) average values for five individual

devices and incident photon-to-current conversion efficiency (IPCE) measurements.
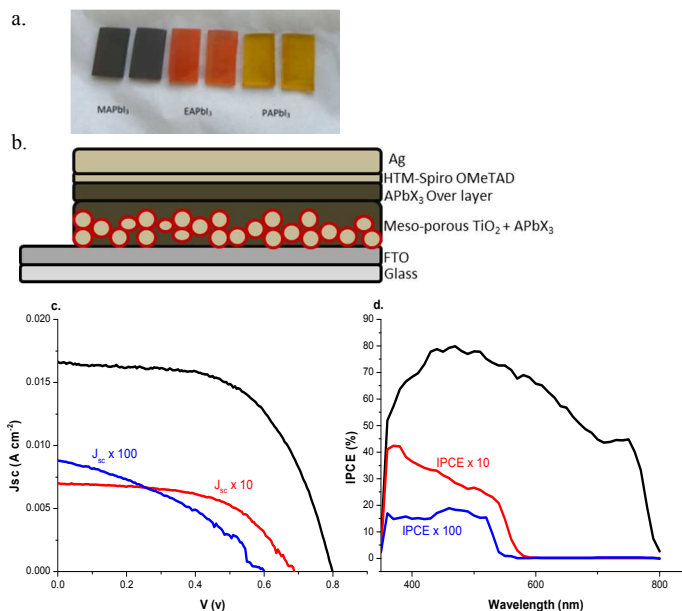
Figure 8. a. Representative photographs of TiO$_2$-substrates spin-coated by the three different alkylammonium lead(II) iodides, APbI$_3$ b. Schematic device architecture for the APbI$_3$-based solar cells c. IV and d. IPCE curves obtained for --- (CH$_3$NH$_3$)PbI$_3$, --- (CH$_3$CH$_2$NH$_3$)PbI$_3$, and ---(CH$_3$CH$_2$CH$_2$NH$_3$)PbI$_3$ based solar cells. IV characterization was done under 1 sun AM1.5G illumination.

Table 3 Photovoltaic parameters (Average values of 5 devices) of the MAPbI$_3$, EAPbI$_3$ and PAPbI$_3$ devices. 600 nm thick TiO$_2$ films were used as substrate, and Spiro-OMeTAD was used as the HTM. A 200 nm layer of silver was used as back contact.

	MAPbI$_3$	EAPbI$_3$	PAPbI$_3$
Jsc mAcm^{-2}	16.29±1.69	0.77±0.14	0.075±0.021
Voc (V)	0.784±0.026	0.662±0.040	0.564±0.034
FF	0.580±0.011	0.521±0.051	0.372±0.034
η (%)	7.4±0.59	0.26±0.025	0.016±0.004
APCE	78.35	2.83	0.18
Band gap(eV)	1.6	2.2	2.4

For the solar cells based on the MAPbI$_3$ as the photosensitizer, a power conversion efficiency of 7.4% was obtained (in our hands). For the EAPbI$_3$ and PAPbI$_3$ sensitized solar cells a dramatic drop in conversion efficiency was observed, 0.26% and 0.02%, respectively. In an effort to reduce the well documented effects of hysteresis,[32] we have scanned all IV curves from positive to negative potentials at a scan rate of 10 mV/s. The IPCE onset for EAPbI$_3$ and PAPbI$_3$ based

solar cells were observed at 550 nm and 525 nm respectively, which are in agreement with the UV-visible spectra. The decrease in efficiency of the $EAPbI_3$ and $PAPbI_3$ solar cells is mainly due to the very low photocurrent of the solar cells. Current density declined from 16.3 mA cm^{-2} for $MAPbI_3$-based solar cell to 0.8 mA cm^{-2} for $EAPbI_3$-based solar cell and 0.075 $mAcm^{-2}$ for $PAPbI_3$-based solar cell. Part of this can be attributed to the increasing bandgap of these materials; the bandgap of $MAPbI_3$, $EAPbI_3$, $PAPbI_3$ were determined to 1.6, 2.2, and 2.4 eV, respectively. However, the Absorbed Photon-to-current Conversion Efficiency (APCE) for each $APbI_3$ material decreases as the alkylammonium cation increases in size, which suggests that the charge-injection or charge-collection is the main limiting factor in these solar cells. Dimensionality may play a significant role as well. $EAPbI_3$ and $PAPbI_3$, which are one-dimensional materials, rather than three-dimensional as $MAPbI_3$, the charge transport ability is much more restricted (as is reflected in their lower electrical conductivities). The lower conductivity exhibited by $EAPbI_3$ and $PAPbI_3$ leads to longer electron transport times in the film and a significantly larger risk of charge recombination for the injected electrons in the conduction band of these materials resulting in decreased charge collection. The APCE values drastically decrease from 78% for $MAPbI_3$ to 3% for $EAPBI_3$ and furthermore to 0.2% for $PAPbI_3$. The APCE decreasing trend is further evidence for the lower efficiency of the solar cells based on the $EAPbI_3$ and $PAPbI_3$. In perovskite-based solar cells, it has been reported that electrons will be carried along the structural lattice of the perovskite material before injection to the oxide semiconductor.[4] There is no reason to believe that another working mechanism is predominant for $EAPbI_3$ or $PAPbI_3$, when compared to the better performing $MAPbI_3$-based solar cells. Previously, $EAPbI_3$ has been used as a quantum-dot photosensitizer in liquid DSC.[29] The low conductivity is likely to not have played a substantial role in such solar cells, since charge transport distances in the $EAPbI_3$ were on the order of the quantum-dot (nanometers) distances instead of 100's of nanometers as in solid-state DSCs. The shorter charge transport distance is likely to lead to a lower risk of charge recombination. This could lead to a significant drop in photocurrent density and the resulting power conversion efficiency.

Conclusions

In order to investigate the structure and function relationships for alkylammonium lead(II) iodides ($APbI_3$), three different $APbI_3$ materials were synthesized with varying bulkiness in the alkylammonium cation (A). From the spectral and structural characterization, we have concluded that by introducing a bulkier cation to the $APbI_3$ materials that the material dimensionality is reduced and that the distance between Pb-I structural units on average increases, both factors result in a substantially lower electrical conductivity. The increase in average distances between lead-iodide structural units is expected to dramatically reduce orbital overlap in $EAPbI_3$ and $PAPbI_3$. The absorption spectra indicate that by moving from $MAPbI_3$ to $PAPbI_3$ that the electronic transitions are shifted to higher energy, which results in weaker absorbance at longer wavelengths. As a consequence, and as expected, an increase in the bandgap of the compounds from 1.6 eV for $MAPbI_3$, 2.2 eV for $EAPbI_3$, and 2.4 eV for $PAPbI_3$ was observed. For $PAPbI_3$ the bulkiness of the cation facilitates the incorporation of solvent molecules into to the crystalline structure. The observed changes in the conductivity of the $APbI_3$ materials are in logical agreement with the structural observations. Solar cells based on these three materials

decreased in efficiency as the length of the alkylammonium cation size increased.

We have provided insight into the key structural properties and their major influences on the physical properties of the $APbI_3$ perovskite-type materials. We have proved that dimensionality is an important factor in obtaining desirable properties from these materials for photovoltaic applications. It has a major effect on the absorption and conductivity, which is highly influential on the functionality of these materials. Crystallographic data of $PAPbI_3$ has been analysed. We have investigated the absorption and conductivity properties of the alkylammonium lead(II) iodide. We have shown that these properties are severely influenced by the structure of these materials. For the first time, $EAPbI_3$ and $PAPbI_3$ have been used in the solid state solar cells. To further improve upon perovskite-like solar cells, this study may offer guidance in the further search to develop new lead-free materials. Further investigations are presently underway to evaluate how the structure of lead-free perovskite-like materials affects their photovoltaic properties.

Acknowledgements

Notes and references

[a] Division of Applied Physical Chemistry, Department of Chemistry, KTH Royal Institute of Technology, SE-100 44, Stockholm, Sweden.
[b] Organic Chemistry, Center of Molecular Devices, Department of Chemistry, KTH Chemical Science and Engineering, 10044, Stockholm, Sweden

† Electronic Supplementary Information (ESI) available: Tables S1, S2, and S3 including detailed crystal structural information of the materials and Figures S1-S3 comparing Raman data for the three $APbI_3$ materials. CCDC 1012805, contain the supplementary crystallographic data for this paper. These data can be obtained free of charge via http://www.ccdc.cam.ac.uk/conts/retrieving.html (or from the CCDC, 12 Union Road, Cambridge CB2 1EZ, UK; fax:441223336033; e-mail: deposit@ccdc.cam.ac.uk)

1. J. Burschka, A. Dualeh, F. Kessler, E. Baranoff, N.-L. Cevey-Ha, C. Yi, M. K. Nazeeruddin and M. Grätzel, *Journal of the American Chemical Society*, 2011, **133**, 18042-18045.
2. S. Mathew, A. Yella, P. Gao, R. Humphry-Baker, F. E. CurchodBasile, N. Ashari-Astani, I. Tavernelli, U. Rothlisberger, K. NazeeruddinMd and M. Grätzel, *Nat Chem*, 2014, **6**, 242-247.
3. H.-S. Kim, C.-R. Lee, J.-H. Im, K.-B. Lee, T. Moehl, A. Marchioro, S.-J. Moon, R. Humphry-Baker, J.-H. Yum, J. E. Moser, M. Gratzel and N.-G. Park, *Sci. Rep.*, 2012, **2**.
4. M. M. Lee, J. Teuscher, T. Miyasaka, T. N. Murakami and H. J. Snaith, *Science*, 2012, **338**, 643-647.

5. K. Akihiro, I. Masashi, T. Kenjiro and M. Tsutomu, *Chemistry Letters*, 2012, **41**, 397.

6. C. R. Kagan, D. B. Mitzi and C. D. Dimitrakopoulos, *Science*, 1999, **286**, 945-947.

7. J. Burschka, N. Pellet, S.-J. Moon, R. Humphry-Baker, P. Gao, M. K. Nazeeruddin and M. Gratzel, *Nature*, 2013, **499**, 316-319.

8. S. D. Stranks, G. E. Eperon, G. Grancini, C. Menelaou, M. J. P. Alcocer, T. Leijtens, L. M. Herz, A. Petrozza and H. J. Snaith, *Science*, 2013, **342**, 341-344.

9. G. Xing, N. Mathews, S. Sun, S. S. Lim, Y. M. Lam, M. Grätzel, S. Mhaisalkar and T. C. Sum, *Science*, 2013, **342**, 344-347.

10. F. Hao, C. C. Stoumpos, D. H. Cao, R. P. H. Chang and M. G. Kanatzidis, *Nat Photon*, 2014, **8**, 489-494.

11. C. C. Stoumpos, C. D. Malliakas and M. G. Kanatzidis, *Inorganic Chemistry*, 2013, **52**, 9019-9038.

12. M. Liu, M. B. Johnston and H. J. Snaith, *Nature*, 2013, **501**, 395-398.

13. N. J. Jeon, J. H. Noh, Y. C. Kim, W. S. Yang, S. Ryu and S. I. Seok, *Nat Mater*, 2014, **13**, 897-903.

14. J.-H. Im, I.-H. Jang, N. Pellet, M. Grätzel and N.-G. Park, *Nat Nano*, 2014, **9**, 927-932.

15. A. Kojima, K. Teshima, Y. Shirai and T. Miyasaka, *Journal of the American Chemical Society*, 2009, **131**, 6050-6051.

16. J.-H. Im, C.-R. Lee, J.-W. Lee, S.-W. Park and N.-G. Park, *Nanoscale*, 2011, **3**, 4088-4093.

17. H. Zhou, Q. Chen, G. Li, S. Luo, T.-b. Song, H.-S. Duan, Z. Hong, J. You, Y. Liu and Y. Yang, *Science*, 2014, **345**, 542-546.

18. T. Baikie, Y. Fang, J. M. Kadro, M. Schreyer, F. Wei, S. G. Mhaisalkar, M. Graetzel and T. J. White, *Journal of Materials Chemistry A*, 2013, **1**, 5628-5641.

19. D. B. Mitzi, M. Yuan, W. Liu, A. J. Kellock, S. J. Chey, V. Deline and A. G. Schrott, *Advanced Materials*, 2008, **20**, 3657-3662.

20. D. B. Mitzi, C. A. Feild, Z. Schlesinger and R. B. Laibowitz, *Journal of Solid State Chemistry*, 1995, **114**, 159-163.

21. D. B. Mitzi, *Journal of Materials Chemistry*, 2004, **14**, 2355-2365.

22. E. Edri, S. Kirmayer, D. Cahen and G. Hodes, *The Journal of Physical Chemistry Letters*, 2013, **4**, 897-902.

23. J. H. Noh, S. H. Im, J. H. Heo, T. N. Mandal and S. I. Seok, *Nano Letters*, 2013, **13**, 1764-1769.

24. I. Borriello, G. Cantele and D. Ninno, *Physical Review B*, 2008, **77**, 235214.

25. G. M. Sheldrick, *University of Göttingen, Germany*, 2003.

26. G. M. Sheldrick, *Acta Crystallographica Section A*, 2008, **64**.

27. J. Tauc, Grigorovici, Radu. and Vancu, Anina, *Phys. Status Solidi B*, 1996, **15**, 10.

28. L. Etgar, P. Gao, Z. Xue, Q. Peng, A. K. Chandiran, B. Liu, M. K. Nazeeruddin and M. Grätzel, *Journal of the American Chemical Society*, 2012, **134**, 17396-17399.

29. J.-H. Im, J. Chung, S.-J. Kim and N.-G. Park, *Nanoscale Research Letters*, 2012, **7**, 353.

30. C. Quarti, G. Grancini, E. Mosconi, P. Bruno, J. M. Ball, M. M. Lee, H. J. Snaith, A. Petrozza and F. D. Angelis, *The Journal of Physical Chemistry Letters*, 2013, **5**, 279-284.

31. S. Michel, A. Courjaud, E. Mottay, C. Finot, J. Dudley and H. Rigneault, *BIOMEDO*, 2011, **16**, 021108-021108-021104.

32. E. L. Unger, E. T. Hoke, C. D. Bailie, W. H. Nguyen, A. R. Bowring, T. Heumuller, M. G. Christoforo and M. D. McGehee, *Energy Environ. Sci.*, 2014, **7**, 3690-3698.